nature nanotechnology

SUPPLEMENTARY INFORMATION

DOI: 10.1038/NNANO.2014.247

An all-in-one nanopore battery array

Chanyuan Liu, Eleanor I. Gillette[†], Xinyi Chen[†], Alexander J. Pearse, Alexander C. Kozen, Marshall A. Schroeder, Keith E. Gregorczyk, Sang Bok Lee[*], and Gary W. Rubloff[*]

1. Surface RuO_2 capacity analysis

We performed a control experiment only with O_3-treated ALD Ru nanotubes in an AAO template without V_2O_5. We measured the capacity of this surface-oxidized Ru material at the same condition as the previous V_2O_5/Ru coaxial nanotube cathode sample. The contribution of the ozone treated Ru to the whole electrode is approximately 18.4 mAh/g at 1C and drops to 5.5 mAh/g at 150C (Figure 3a). Because electrical double layer capacity contribution will remain nearly constant from low to high C rates[1], its contribution will be no more than 5.5 mAh/g. X-ray photoelectron spectroscopy (XPS) measurement estimated the thickness of RuO_2 on Ru surface as 3.4nm, which indicates RuO_2 to V_2O_5 mass ratio to be 0.595. Considering the excess capacity from RuO_2 as 12.9mAh/g (18.4 – 5.5 mAh/g), we can estimate the specific capacity of RuO_2 within 4V to 2.6V to be about 22 mAh/g at 1C rate. This can be easily understood from the fact that the electrochemical lithiation of RuO_2 occurs mainly below 2.1V vs. Li/Li^+,[2] meaning there will be little electrochemical faradaic reaction in the potential range 4 - 2.6V. Therefore, while there is some electrochemical reaction from the Ru nanotube, its contribution to the overall capacity is very small and it plays mainly an important role as a high-conductivity, conformal current collector.

Detailed XPS analysis is presented as follows, which reveals approximately 3.4nm of RuO_2 is present between the Ru and V_2O_5 with ±1nm error. We fabricated a planar model system of 7.5nm of ALD Ru followed by 2nm of ALD V_2O_5 on a quartz substrate and XPS to explore the chemistry of the buried Ru current collector. Presumably, any oxidation of the Ru stops when the surface is completely passivated by vanadium oxide.

All data were collected on a Kratos AXIS Ultra DLD instrument using monochromated Al Kα x-rays (1486.6 eV) as the excitation source. The x-ray source was operated at 12 kV with 12 mA current for all measurements, and the analyzer was operated in hybrid (magnetic immersion) mode using the slot aperture. High resolution spectra were collected using pass energy 20 and a 0.05 eV step size. Due to the conformal nature of the Ru film on the quartz substrate, the sample was conductively coupled to the sample holder of the XPS use of the charge neutralizer was not required. The sample was briefly

exposed to a low intensity beam of 1keV Ar+ ions in order to remove surface carbon from air exposure, as the C 1s peak overlaps with the Ru 3d region of interest. We do not believe this ion beam exposure significantly affected the Ru current collector because it removed less than half of the 2nm V_2O_5 overlayer.

Peak fitting of the Ru 3d region was performed using CasaXPS. The background was fit with a Shirley linetype, and all component peaks were 30% Lorenztian Voigt functions multiplied by an asymmetric exponential tail to high binding energy because both Ru and RuO_2 are metallic conductors. Ru 3d spectra are in general quite complicated, and each spin component in this case required 3 peaks to fit: once associated with Ru^0 (peak 1 in Figure S1), one associated with Ru^{4+} (peak 2), and one also associated with Ru^{4+} but shifted to a higher binding energy (peak 3). This third feature is most likely due to final state screening[3] in the conductive oxide. The peak separation between the $Ru^0(5/2)$ and $Ru^0(3/2)$ peaks was constrained to be 4.2 eV following literature values[4, 5]. All FWHMs were constrained to be below 3eV because of the high background and the tendency of the fitting algorithm to overbroaden, and the area ratios between the 5/2 and 3/2 spin components were constrained to match the theoretical value of 3:2. These constraints resulted in a fit which did not require the addition of a C 1s peak, with peak locations in excellent agreement with literature[3, 4, 5], and confirmed the presence of a significant amount of RuO_2, though the surface RuO_2 contribute little to battery capacity at the voltage rage of 4V to 2.6V.

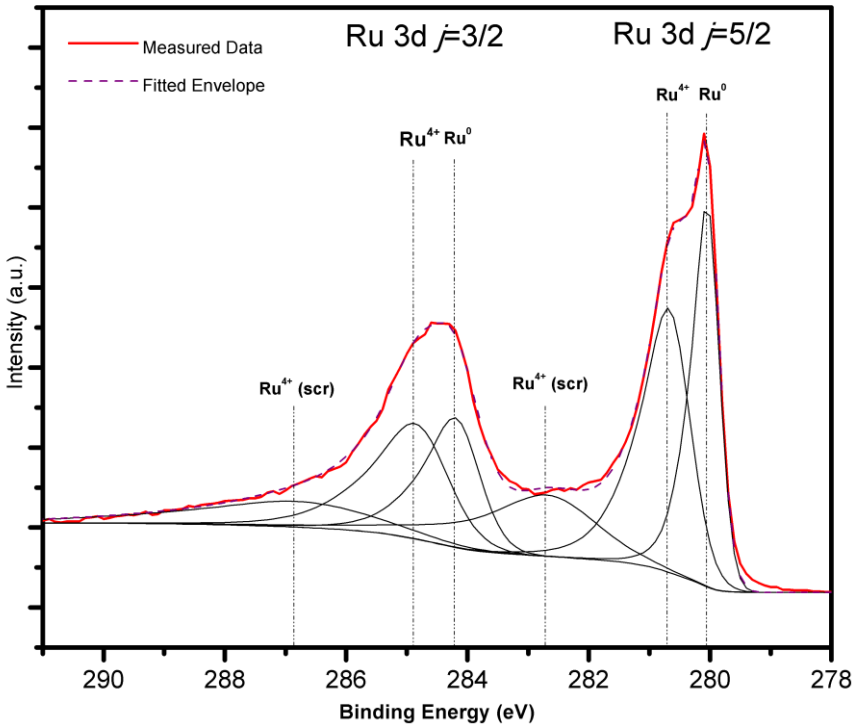

Figure S1| XPS data for analyzing RuO2 thickness. The photoemission spectrum of the Ru 3d core level region. Each spin component is fit with three peaks: Ru(0) corresponding to metallic Ru, Ru(4+) referring to ruthenium dioxide, and Ru(4+) (scr) referring to a further contribution from the ruthenium dioxide arising from final state screening.

We estimated the thickness of the oxide layer following the procedure developed by Ernst and Sloof[6], except using the Ru 3d region instead of the Ru 3p region. Assuming the Ru substrate and oxide are flat and homogenous, the ratio R of the oxide to metal component peak areas is

$$R = \frac{C_{RuOx}\lambda_{Ru(3d),ox}}{C_{RuMet}\lambda_{Ru(3d),met}}\left\{ e^{\left(\frac{d}{\lambda_{Ru(3d),ox}\sin\theta}\right)} - 1 \right\}$$

Where $\frac{C_{RuOx}}{C_{RuMet}}$ is the ratio of the concentration of Ru atoms in the oxide and the metal, taken to be approximately 1/3, θ is the angle between the substrate and the analyzer (0 in this case), and d is the thickness of the oxide. $\lambda_{Ru(3d),ox}$ and $\lambda_{Ru(3d),met}$ are the inelastic mean free paths of Ru 3d photoelectrons (kinetic energy of 1206eV when excited with Al Kα x-rays) in the oxide and metal, respectively. These latter two parameters were calculated using the QUASES-IMFP-TPP2M software package (http://www.quases.com/products/quases-imfp-tpp2m/) to be 1.99nm in the oxide and 1.65nm in the metal. R can then be calculated based on our peak fitting by taking the area ratio of both oxide peaks from the 5/2 spin component (peaks 2 and 3) and the metallic 5/2 component (peak 1), and we find $R = 1.87$. Solving the above equation for d then yields $d = 3.4$nm. Realistically, this value should be taken to be ±1nm considering error inherent in complex peak fitting, although d is relatively insensitive to R because of the logarithmic dependance. It is important to note that this analysis is unaffected by the presence of a V_2O_5 overlayer because all signal from both the metallic and oxide layer would be retarded by the same amount, preserving R.

2. COMSOL finite element simulation

To understand the contribution of the ruthenium as a nanostructured current collector, a finite element model was developed to predict the behavior of nanostructured V_2O_5 half cells. COMSOL Multiphysics' lithium ion battery module was used to perform these simulations, which were calculated for a single pore, with an electrolyte reservoir with a surplus of lithium available. The pore is 10 µm long, with a

radius of 75nm. The active material occupies the outer 30nm of the pore, with a mass of 3.8 x 10^{-7} µg. The active material has a conductivity of 0.005 S m^{-1} and a lithium diffusion constant of 3 x 10^{-17} m^2s^{-1}. Built in parameters for 1M $LiPF_6$EC/DEC electrolyte are used for the electrolyte conductivity, lithium transport number and diffusion coefficient. The material potential is calculated as a function of the lithium concentration in the active material, as determined by the current-voltage relationship in a planar V_2O_5 film at a very slow rate. Only galvanostatic discharge is modeled for this study, so the initial conditions assume 4.0V on the cathode, with only 1 mM Li present in the active material. As current is applied, the electrode potential changes as a function of inserted lithium concentration, based on a discharge curve measured at a C/3 rate for a planar V_2O_5 electrode fabricated by ALD on a stainless steel disc. Discharge time is defined as the time required for the average potential on the electrode to drop to 2.60 V. To simulate discharge, total current is calculated from the mass and the theoretical capacity, and is applied either along the bottom boundary of the active material, or along the entire outside surface of the pore. In this way, the models simulate only a difference in current collector, without accounting for any material or geometry changes related to the fabrication of the real devices.

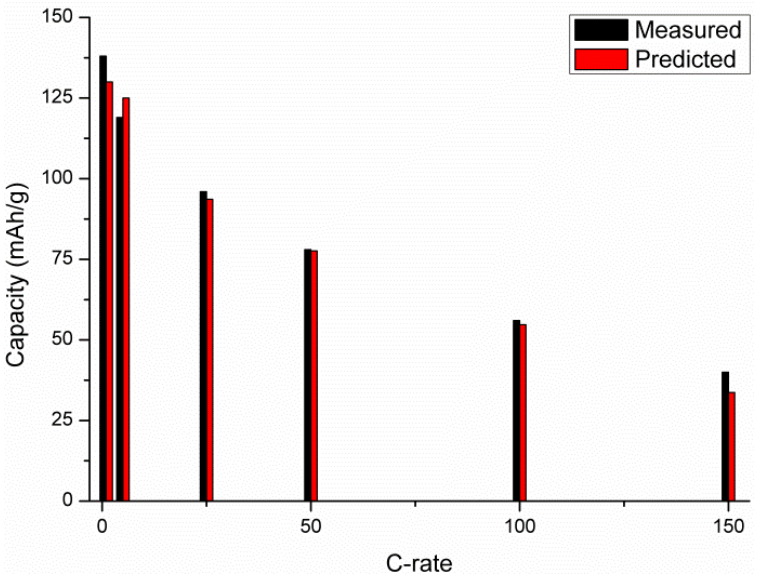

Figure S2| Comparison of predicted and measured capacity of a V_2O_5 half cell with a planar current collector. The predicted gravimetric capacity values from COMSOL simulation match well with measured values from 1C to 150C.

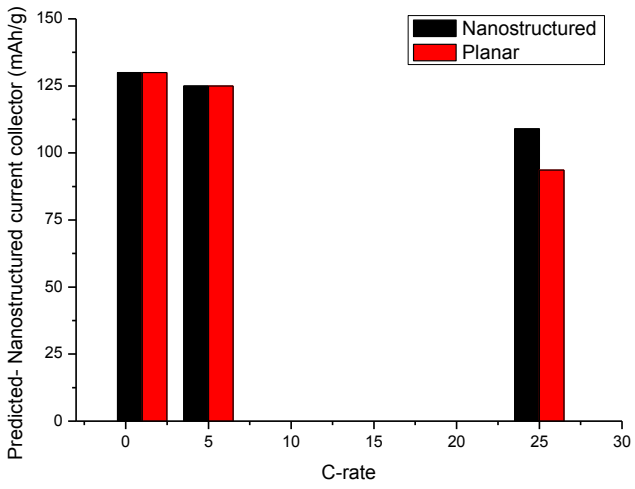

Figure S3| Comparison of predicted capacity of a V_2O_5 half cell with planar and nanostructured current collectors. The predicted gravimetric capacity values from COMSOL simulation match well with measured values from 1C to 25C.

3. Deconvoluting charge from CV as a function of scan rate

The CVs can be used to probe the kinetics of the overall reaction, and quantify the contribution of fast, surface-dominant reactions as well as slower, diffusion insertion-dominant reactions to the total charge stored. Generally, the surface-dominant reaction charge includes the electrical double layer and contribution from fast faradaic reactions on the exposed electrode surface. The insertion-dominant charge is generally the contribution from bulk Li insertion. These two contributions can be distinguished by their kinetics. Typically the slower insertion-dominant reaction current scales linearly to the square root of the scan rate ($\upsilon^{1/2}$), unlike surface-dominant reaction current, which scales linearly to the scan rate (υ). Because of this difference in scan rate dependence, the two contributions can be separated mathematically.

There are two methods commonly used in the literature to deconvolute surface and bulk charge in energy storage electrodes using cyclic voltammetry. Both methods rely on the fundamental concept that the surface and bulk of a material are governed by different kinetics, and will respond differently to increasing scan rates. However, each method takes a different mathematical approach to differentiate between the two. Trasatti's method[7] estimates the charge at a theoretical scan rate of 0, which

corresponds to the maximum total charge possible at an infinitely slow scan rate, by plotting (1/Q) vs. the square root of the scan rate. The y-intercept of the linear region of the plot is $1/Q_{total}$. (Figure S5b and S8b) Then, to extract the surface charge, the charge is extrapolated to an infinitely fast scan rate by plotting charge vs. $v^{-1/2}$. The y-intercept is the surface charge, corresponding to a scan rate of infinity where it is assumed all bulk contributions are eliminated. (Figure S5a and S8a)

The second method of deconvoluting surface and bulk charge has been described in detail in the literature by Dunn and coworkers[8]. This method deconvolutes the surface and bulk contributions to current at a given voltage, i(V), based on the following equation:

$$i(V) = k_1 v + k_2 v^{1/2}$$

When rearranged, this equation can be plotted with $i/v^{1/2}$ as a function of $v^{1/2}$, providing k1 and k2 as the slope and intercept respectively.

$$\frac{i(V)}{v^{1/2}} = k_1 v^{1/2} + k_2$$

Determining this ratio for 100 points during each sweep of the CV can provide the plots seen in Figure S6. However, the peak shifts, especially at high scan rates, introduce error to these calculations that makes to more valuable as qualitative indicators that even the redox peak regions are behaving like surface charge regions, scaling linearly with the scan rate. This provides evidence that the nanotube architecture presented here facilitates fast ion transport by minimizing ion diffusion lengths.

a) V_2O_5 with 3d Ru current collector

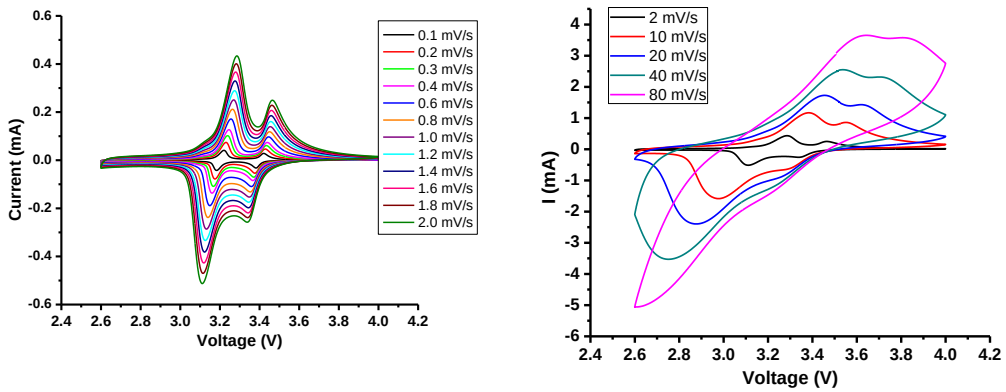

Figure S4| CV of V_2O_5 with Ru nanotube current collectors at different scan rate cycled inside a coin cell against Lithium metal. (Left panel: 0.1mV/s-2.0mV/s, right panel:2mV/s-80mV/s). The CV curves show obvious ion insertion peaks up to 80mV/s.

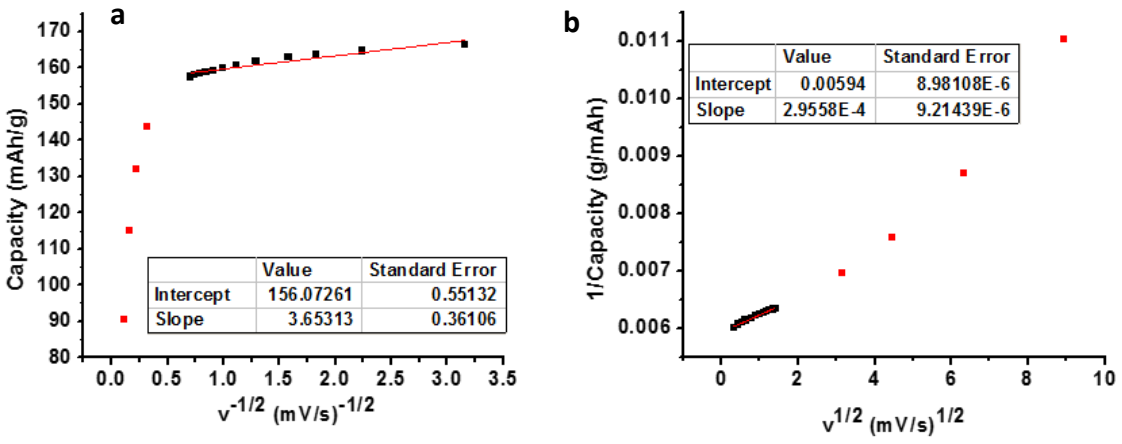

Figure S5| Trasatti's method for V_2O_5 with Ru nanotube current collectors. **a** Gravimetric capacity versus inverse square root of scan rate for V_2O_5/Ru nanotube arrays. The Intercept value represents the charge proportional to scan rate (v), which is 156.1 mAh/g. **b** Inverse gravimetric capacity versus square root of scan rate for V_2O_5/Ru nanotube arrays. The inverse of the intercept value is the total charge (168.4 mAh/g).

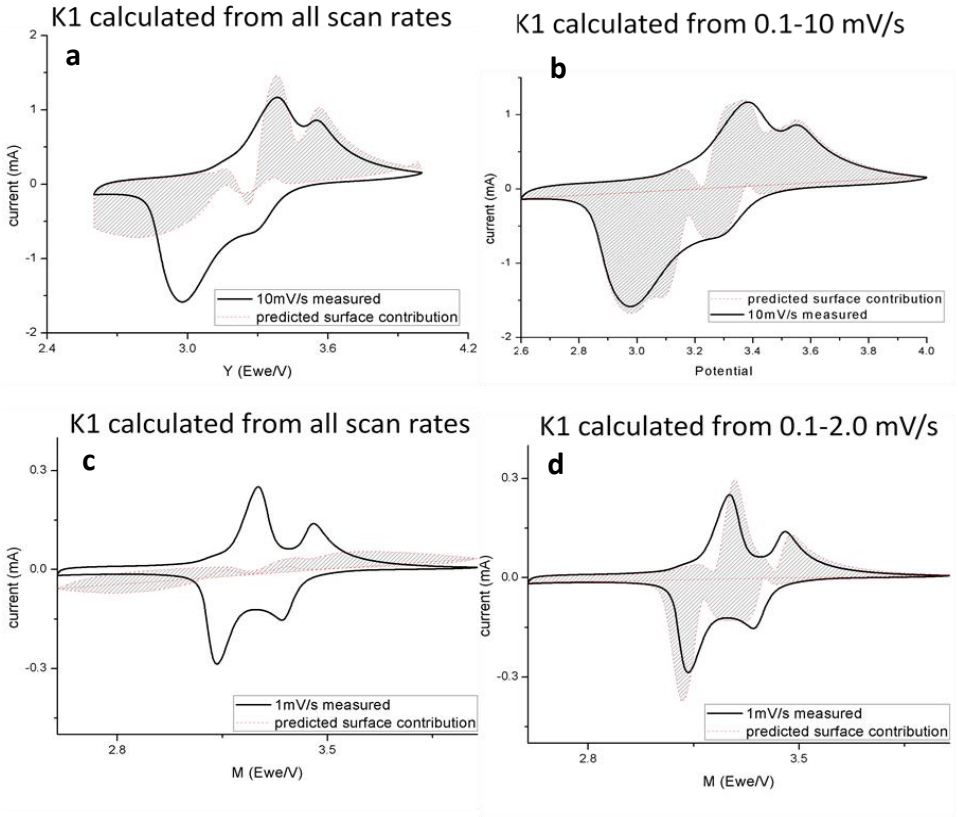

Figure S6|v –dependent charge by Dunn's method at different scan rates. Solid black lines are measured CV curve. The gray shaded areas indicate the calculated v –dependent charge based on coefficient k1. **a** and **b** actual CV curve measured at 10mV/s and the v –dependent charge based on a k1, which is fitted by the CV curves from all scan rates and from 0.1 mV/s to 10mV/s, respectively **c** and **d** actual CV curve measured at 1mV/s and the v –dependent charge based on a k1, which is fitted by the CV curves from all scan rates and from 0.1 mV/s to 10mV/s, respectively.

a) V_2O_5 with planar Au current collector

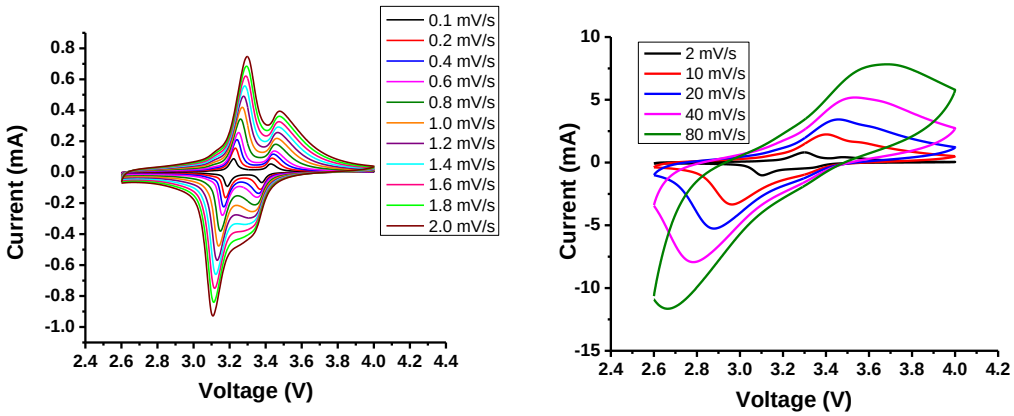

Figure S7| CV of V_2O_5 with planar Au current collectors at different scan rate cycled inside a coin cell against Lithium metal (Left panel: 0.1mV/s-2.0mV/s, right panel:2.0mV/s-80mV/s). The absolute current values are larger than the ones of V_2O_5/Ru nanotube, which results from the larger total mass of V_2O_5 in V_2O_5/planar Au cathode. However, its current normalized by V_2O_5 mass is smaller than that of V_2O_5/Ru nanotube. The two sets of peaks at ~3.2V and ~3.4V, corresponding to lithium ion insertion, merge together and can't be distinguished when scan rate is larger than 10 mV/s.

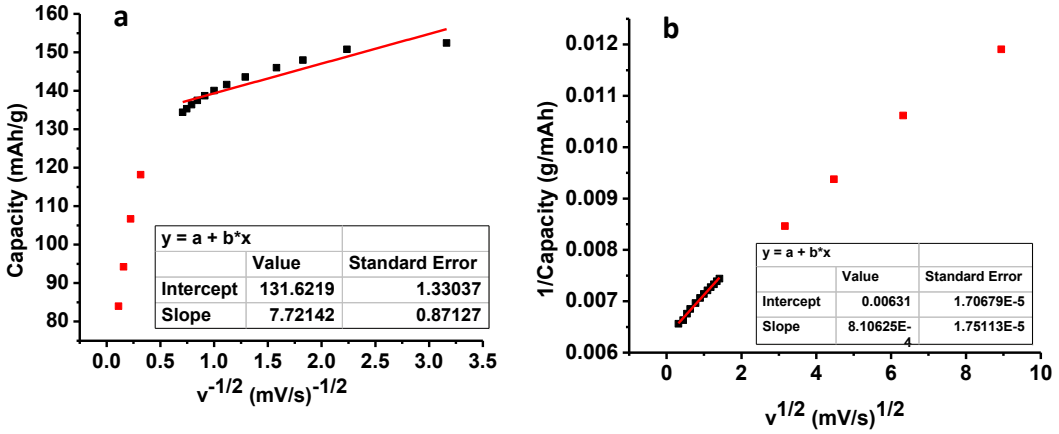

Figure S8| Trasatti's method for V_2O_5/Au cathodes. a Gravimetric capacity versus inverse square root of scan rate. The Intercept value represents the charge proportional to scan rate (v), which is 131.6 mAh/g. **b** Inverse gravimetric capacity versus square root of scan rate. The inverse of the intercept value is the total charge 158.5 mAh/g.

4. Scaling up power and energy density by device geometry optimization

Table S1 Device Radius Measurement. The radii of AAO template, area coated with Ru and area coated with both Ru and V_2O_5 are measured by counting the pixels in inside each area. The radius of AAO template is known as 0.65cm.

Features	Radius (pixel)	Actual Radius (cm)
AAO	286	0.65
Ru	251	0.57
V_2O_5+Ru	139.75	0.32

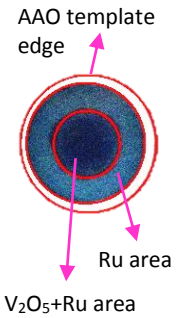

Table S2 Device Geometry summary

Device Radius (cm)	0.318
AAO template thickness (um)	50
pore diameter (nm)	150
pore period (nm)	251
V_2O_5 depth (nm)	6000
V_2O_5 thickness (nm)	21
V_2O_5 density (ug/(cm^2um))	336

Table S3 Cell geometry optimization for higher volumetric energy and power density

		Current geometry	Optimization1	Optimization2[9]
pore diameter (nm)		150	100	75.3
pore period (nm)		251	150	96.6
V_2O_5 depth (nm)		6000	12000	12000
V_2O_5 thickness (nm)		21	18	15
porosity		32 %	40 %	55%
active material mass/volume (ug/cm2um)	Calculated	7.4	23.5	35.5
	Actual	3.7	N/A	N/A
1C power density (uW/(um·cm^2))		0.49	3.2	4.8
1C energy density (uWh/(um·cm^2))		0.60	3.8	5.8
150C power density (uW/(um·cm^2))		52	335	506
150C energy density (uWh/(um·cm^2))		0.19	1.2	1.9

*Assume power and energy density linearly increase with mass loading per volume

If the battery output potential is doubled to 2V by replacing the anode side with other low voltage materials like TiO_2 or SnO_2, the total energy and power density could potentially be increased to 2X based on the results of optimization2, reaching 3.8 $\mu Wh\mu m^{-1}cm^{-2}$ and 1012 $\mu W\mu m^{-1}cm^{-2}$.

5. Li ion path (Leakage current path)

Since nanotube battery arrays are immersed in electrolyte, there are two possible paths for Li ions, one is through AAO nanopores, and the other is around the edge of AAO template. We sputtered more than 1µm Au at the back of a half cell (V_2O_5 cathode with Ru integrated current collector) to block the pores to limit lithium ion diffusion in the circuit path around AAO edge. The trend of capacity variation at different C rate of this control sample is comparable to regular half-cell results described in the article, though the absolute value is less, which may result from part of V_2O_5 blocked from electrolyte contact by thick Au layer.

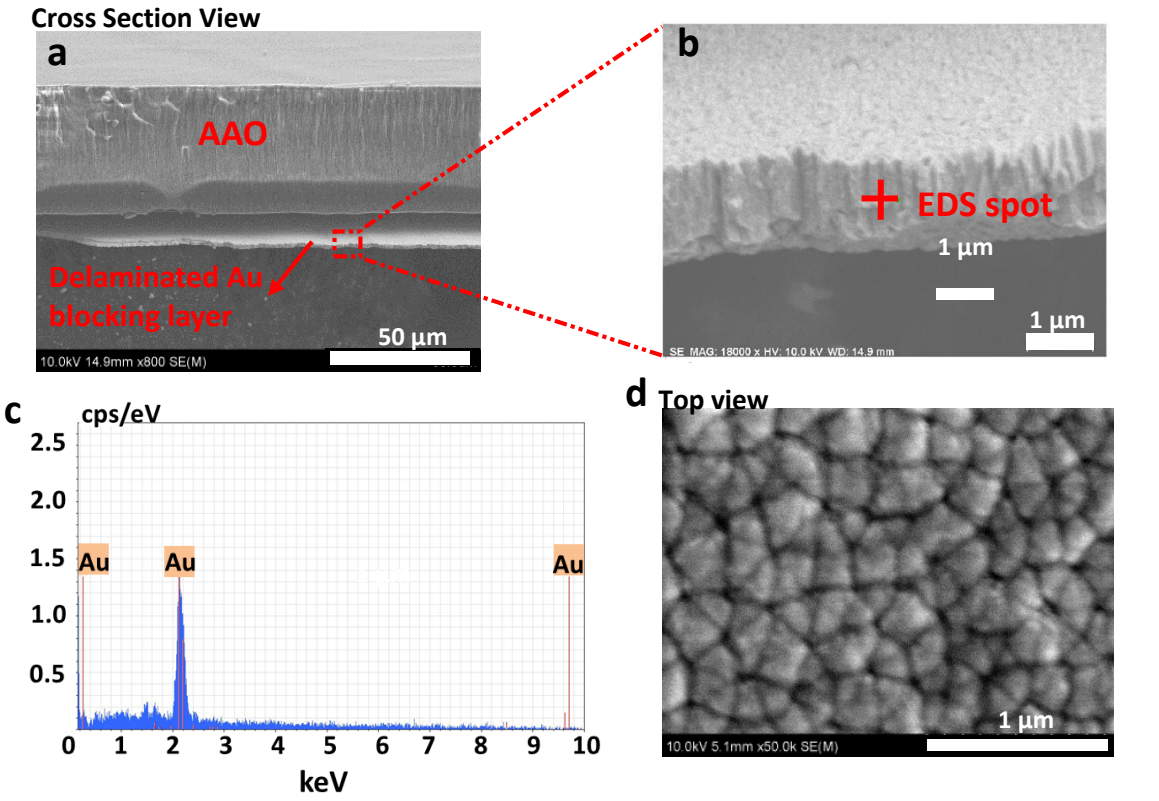

Figure S9| SEM images showing about 1um thick Au layer blocking AAO pores. **a** Cross section view of a V_2O_5/Ru nanotube current collector half cell device with a thick Au layer for blocking electrolyte path. The Au layer is delaminated from the cathode for a clear view. **b** Zoom in image of Au blocking layer, which is more than 1 µm thick. **c** EDS spectrum at the position marked in b confirms the delaminated layer is Au. **d** Top view of the device shows AAO pores are blocked by the thick gold layer.

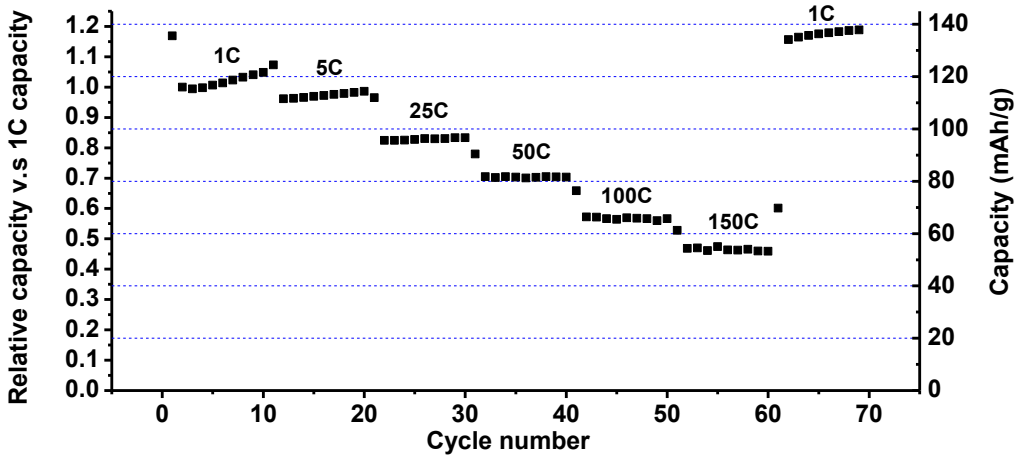

Figure S10| Rate performance of a V_2O_5/Ru integrated current collector, with pores blocked at the back side. The retention rate at different cycling rate is comparable to the ones without blocking the pores.

6. Degradation of V_2O_5.

A half cell was opened after rate testing and aging in electrolyte for more than 6 months. The electrode was found without any crack after reopening the coin cell and was washed by dimethoxyethane (DME) to clean the residue organic electrolyte before SEM testing. It still shows a strong vanadium signal in SEM EDS elemental mapping, revealing around 6μm depth vanadium oxide remaining in the pores (similar to the as-prepared measurement) after cycling (Figure S11). No visible morphology changes were observed after cycling. Notably, the AAO membrane remained unbroken after reopening the coin cell, which demonstrates the mechanical robustness of AAO during processing.

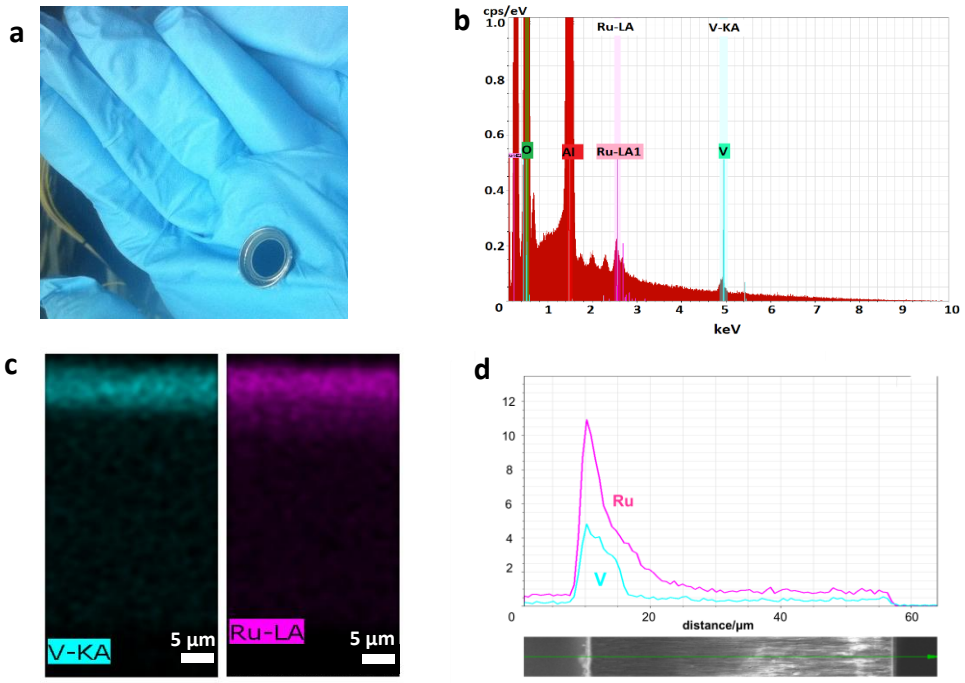

Figure S11| half cell after cycling. a Intact half cell after cycling and reopening the coin cell, indicating the mechanical robustness of the device. **b** EDS spectrum indicates strong vanadium signal (blue). **c** and **d** elemental mapping and line scan both indicate around 6µm depth vanadium oxide remaining in AAO pores.

7. Explanation to the capacity drop at the ~60th cycle in the asymmetrically cycled full cell.

The step function decrease in capacity happened at the 60th cycle. During battery cycling, it was stopped at the 60th cycle and left open circuit for 65 hours. It was found that the open circuit voltage almost didn't change during this period (stopped at 0.57V and measured to be 0.60V after 65 hours). When we resumed cycling of the battery, we noted a modest capacity loss (~5%) after the 65 hours of open circuit. (In fact the cycle life of this battery could have been even longer without this long rest period.)

Other Information

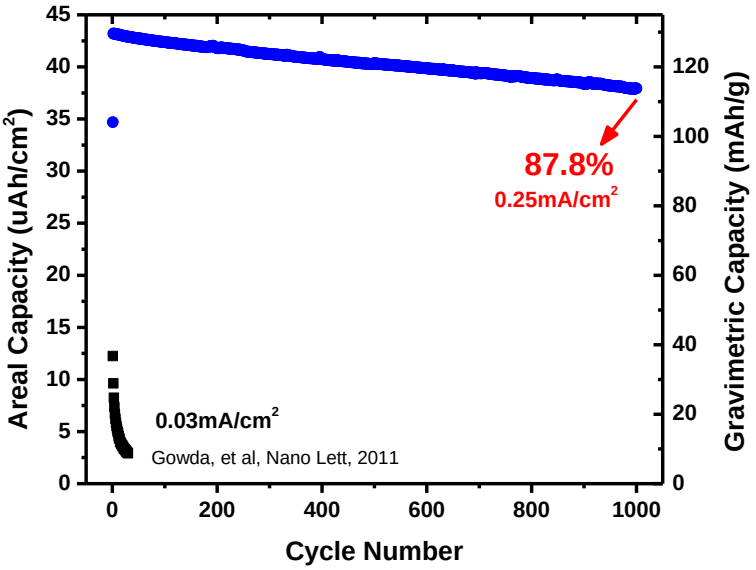

Figure S12| 4X Capacity with 30X life time at 10X current density comparing to other full cell structure built inside AAO pores.

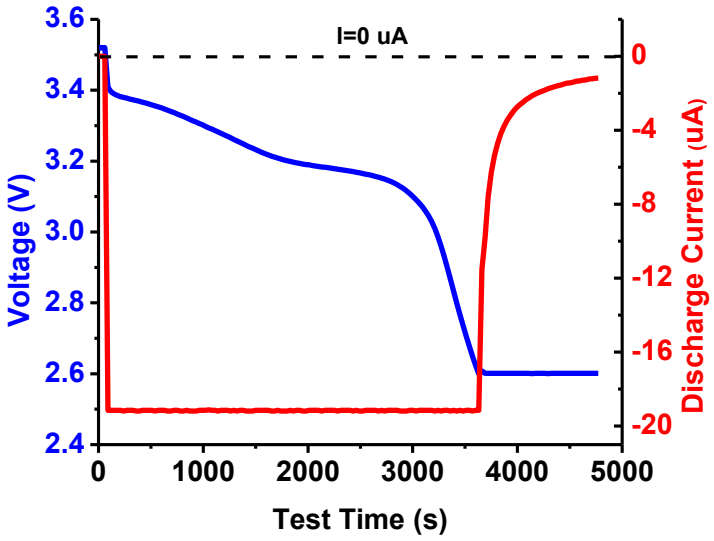

Figure S13| Anode prelithiation diagram

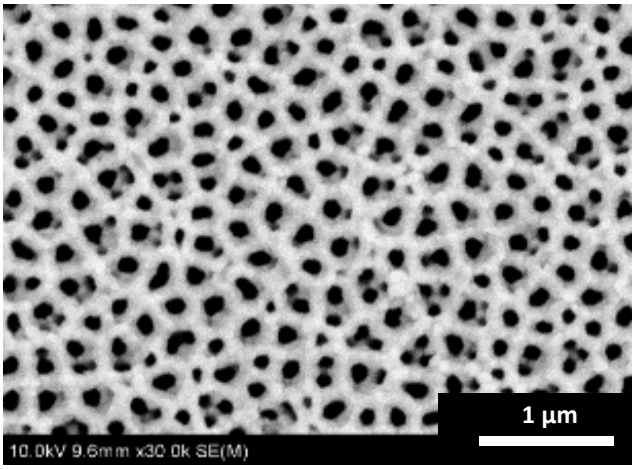

Figure S14| SEM top view of V_2O_5/Au cathode with thin layer of sputtered Au as planar current collector leaving AAO pores open. Planar current collector has similar resistance with integrated current collector on the top surface, but their electrical conductivity along vertical direction deep into V_2O_5 nanotubes are different.

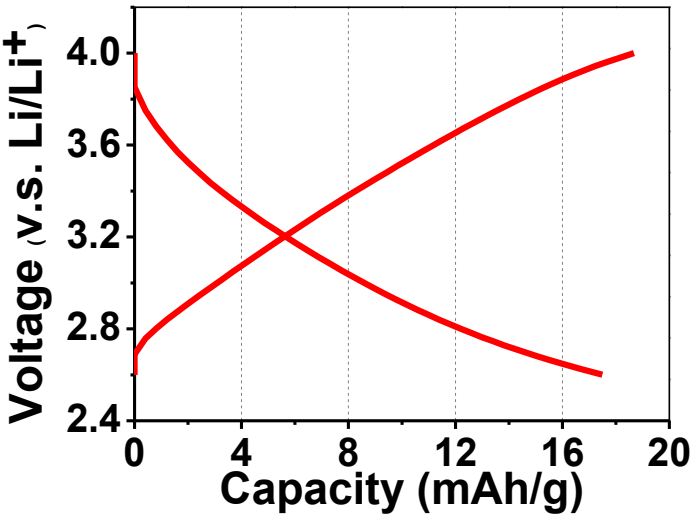

Figure S15| galvanostatic charge/discharge curves of Ru coated AAO with O3 treatment cycled at 1C within voltage range 4-2.6V.

References

1. Winter M, Brodd RJ. What are batteries, fuel cells, and supercapacitors? *Chemical Reviews* 2004, **104**(10)**:** 4245-4269.

2. Hu Y-Y, Liu Z, Nam K-W, Borkiewicz OJ, Cheng J, Hua X*, et al.* Origin of additional capacities in metal oxide lithium-ion battery electrodes. *Nature Materials* 2013, **12**(12)**:** 1130-1136.

3. Cox PA, Goodenough JB, Tavener PJ, Telles D, Egdell RG. THE ELECTRONIC-STRUCTURE OF BI2-XGDXRU2O7 AND RUO2 - A STUDY BY ELECTRON-SPECTROSCOPY. *Journal of Solid State Chemistry* 1986, **62**(3)**:** 360-370.

4. Rochefort D, Dabo P, Guay D, Sherwood PMA. XPS investigations of thermally prepared RuO2 electrodes in reductive conditions. *Electrochimica Acta* 2003, **48**(28)**:** 4245-4252.

5. Shen JY, Adnot A, Kaliaguine S. AN ESCA STUDY OF THE INTERACTION OF OXYGEN WITH THE SURFACE OF RUTHENIUM. *Applied Surface Science* 1991, **51**(1-2)**:** 47-60.

6. Ernst MA, Sloof WG. Unraveling the oxidation of Ru using XPS. *Surface and Interface Analysis* 2008, **40**(3-4)**:** 334-337.

7. Ardizzone S, Fregonara G, Trasatti S. “Inner” and “outer” active surface of RuO2 electrodes. *Electrochimica Acta* 1990, **35**(1)**:** 263-267.

8. Wang J, Polleux J, Lim J, Dunn B. Pseudocapacitive contributions to electrochemical energy storage in TiO2 (anatase) nanoparticles. *J Phys Chem C* 2007, **111**(40)**:** 14925-14931.

9. Ersching K, Dorico E, da Silva RC, Zoldan VC, Isoppo EA, Viegas ADC*, et al.* Surface and interface characterization of nanoporous alumina templates produced in oxalic acid and submitted to etching procedures. *Materials Chemistry and Physics* 2012, **137**(1)**:** 140-146.